THE JOURNAL OF PHYSICAL CHEMISTRY B
A JOURNAL OF THE AMERICAN CHEMICAL SOCIETY

pubs.acs.org/JPCB

Article

Upconversion $NaYF_4$:Yb^{3+}/Er^{3+}@silica-TPGS Bio-Nano Complexes: Synthesis, Characterization, and *In Vitro* Tests for Labeling Cancer Cells

Tran Thu Huong,* Ha Thi Phuong, Le Thi Vinh, Hoang Thi Khuyen, Do Thi Thao, Le Dac Tuyen, Tran Kim Anh, and Le Quoc Minh

Cite This: *J. Phys. Chem. B* 2021, 125, 9768–9775

Read Online

ACCESS | Metrics & More | Article Recommendations

ABSTRACT: Fluorescence imaging is an important technique used for early diagnosis and effective treatment of some incurable diseases including cancer. Herein, we report novel $NaYF_4$:Yb^{3+}/Er^{3+}@silica-TPGS bio-nano complexes for labeling cancer cells. The $NaYF_4$:Yb^{3+}/Er^{3+} nanoparticles have been successfully synthesized *via* a hydrothermal route, further coated with a silica shell, and functionalized with D-α-tocopheryl polyethylene glycol 1000 succinate (TPGS). The experimental results indicate that $NaYF_4$:Yb^{3+}/Er^{3+}@silica-TPGS emits stronger upconversion luminescence than $NaYF_4$:Yb^{3+}/Er^{3+} under an excitation of 980 nm. More significantly, the $NaYF_4$:Yb^{3+}/Er^{3+}@silica-TPGS bio-nano complexes could strongly label MCF-7 breast cancer cells for *in vitro* experiments detected by a fluorescence microscope. On the other hand, the complex could not typically probe healthy cells, which are HEK-293A human embryonic kidney cells, under the same experimental conditions. Because of their strong upconversion luminescence, good dispersibility, and biocompatibility, $NaYF_4$:Yb^{3+}/Er^{3+}@silica-TPGS bio-nano complexes can be a promising candidate/probe for biomedical labeling and diagnostics.

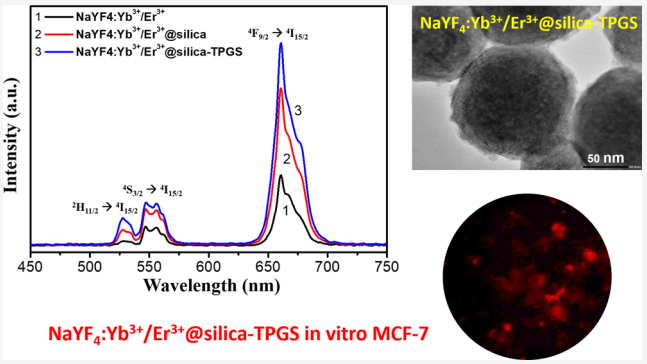

INTRODUCTION

Fluorescence imaging using down/upconversion nanomaterials is one of the most important techniques used in noninvasive and high-sensitivity biomedical diagnostics.[1−5] It is very useful for the early diagnosis and treatment of some incurable diseases. Recently, fluorescence labeling techniques have been developed and utilized for humans.[1] Because of their unique optical properties, upconversion luminescence nanomaterials doped with rare-earth (RE) ions could be used to label biotissues and cells.[6,7] The RE ions exhibit strong luminescence and excellent photostability and are composed of materials that are nontoxic to biological organisms.[8−11] Furthermore, excitation at long wavelengths (near-infrared (NIR) and IR) also allows for deeper tissue penetration and minimizes damage to biological samples. Especially, it can eliminate autofluorescence from biotissues and increase accuracy for *in vivo* and *in vitro* bioimaging.[6,7,12−14]

The RE ions of Yb^{3+} and Er^{3+} codoped nanomaterials have been most used to obtain upconversion luminescence, mainly due to the large absorption cross section of around 980 nm in Yb^{3+}, the relative long luminescence lifetime of Er^{3+}, and the good energy level match between the two RE ions.[14−17] The host materials are usually based on inorganic matrices with low phonon energy, such as oxides, vanadates, phosphates, borates, and fluorides.[17−21] We also know that RE-doped fluoride ($NaYF_4$) compounds possessing the lowest phonon energy have been regarded as currently one of the most excellent upconversion materials. Furthermore, exploration of $NaYF_4$:Yb^{3+}/Er^{3+} compounds for their biological applications is still less developed. However, their surface is protected by hydrophobic ligands, and needs to modify and functionalize for good stability, dispersibility, and biocompatibility.[15−17]

To solve this practical problem, an amphiphilic surfactant is used to convert the hydrophobic upconversion nanomaterials into hydrophilic ones with prolific chemically reactive groups, leading to increased aqueous dispersion and biocompatibility.[3,14,15] More interestingly, D-α-tocopheryl poly(ethylene glycol) 1000 succinate (TPGS), a water-soluble derivative of natural vitamin E, has multiple advantages and is widely applied in food and drug delivery.[22,23] The TPGS molecule is

Received: June 21, 2021
Revised: August 10, 2021
Published: August 20, 2021

an amphiphilic structure with a hydrophilic polar head portion and a lipophilic alkyl tail. This enables TPGS to be used as a surfactant to encapsulate hydrophobic drugs and to act simultaneously as a solubilizer, emulsifier, absorption enhancer, and antioxidant.[23,24] Thus, TPGS is an extensive area of current research on drug delivery systems. However, the investigation on the bio-nano complex probes of TPGS is lacking and still in progress.

In this paper, we report the achievements in synthesis and testing of $NaYF_4$:Yb^{3+}/Er^{3+}@silica-TPGS bio-nano complexes as a tool for labeling cancer cells. Upconversion luminescence nanomaterials $NaYF_4$:Yb^{3+}/Er^{3+} were synthesized *via* a hydrothermal route, further protected with a silica shell, and then functionalized with TPGS. The upconversion optical properties are discussed in detail. We also evaluated *in vitro* bioimaging of MCF-7 breast cancer cells and HEK-293A embryonic kidney cells using a fluorescence microscope.

MATERIALS AND METHODS

Preparation of $NaYF_4$:Yb^{3+}/Er^{3+} Nanoparticles. $Y(NO_3)_3{\cdot}6H_2O$ (99.9%), $Yb(NO_3)_3{\cdot}5H_2O$ (99.9%), $Er(NO_3)_3{\cdot}5H_2O$ (99.9%), and NaF (99%) were purchased from Sigma. NaOH (99%) and trisodium citrate dihydrate $HOC(COONa)(CH_2COONa)_2{\cdot}2H_2O$ (99%) were provided by Merck. All chemicals were of analytical grade and used without further purification. In a typical synthesis of $NaYF_4$:Yb^{3+}/Er^{3+} nanoparticles, the salts of $Y(NO_3)_3$, $Yb(NO_3)_3$, and $Er(NO_3)_3$ were mixed with a molar ratio of 79.5/20.0/0.5 using a magnetic stirrer. Then, trisodium citrate dihydrate, sodium hydroxide, and diethylene glycol (DEG) were slowly added and stirred for 1 h (solution 1). After that, sodium fluoride was poured into solution 1 and stirred for 2−3 h. The mixture was transferred to a 100 mL Teflon-lined autoclave and heated at 200 °C for 10−24 h. After the hydrothermal reaction, the autoclave cooled down naturally to room temperature. The precipitates were separated by centrifugation at 5800 rpm for 10 min, washed several times in water, and dried in air at 60 °C for 24 h.

Surface Modification and Functionalization. Surface modification of $NaYF_4$:Yb^{3+}/Er^{3+} upconversion nanoparticles not only improves photostability of the nanoparticles with desirable interfacial properties but also provides a potential platform for attaching biological macromolecules for various biomedical applications.[25−29] Furthermore, the biomedical labels need to have a specific property to target a specific tumor such as its surface must have suitable ligands that link to the cells. So, we covered the upconversion nanoparticle surface with a silica shell by the Stöber method. Silica is one of the ideal materials for surface modification of $NaYF_4$:Yb^{3+}/Er^{3+} nanoparticles because of its high biocompatibility, water solubility, and high stability, and it can avoid the potential toxicity of precursors to cells. Silica has been used to cover the surface of the upconversion nanoparticles through the formation of Si−O−Si bonds and OH groups. Then, these upconversion nanoparticles were added to TPGS to link biomolecules to the surface of nanomaterials.

Briefly, 10 mL of $NaYF_4$:Yb^{3+}/Er^{3+} solution was added to a mixture solution containing 10 mL of tetraethyl orthosilicate in absolute ethanol, deionized water, and acetic acid and stirred for 24 h at room temperature by a magnetic stirrer. The solution was then centrifuged and washed several times with 50% ethanol solution. Final products of $NaYF_4$:Yb^{3+}/Er^{3+}@silica nanoparticles were dried at 60 °C for 24 h in air.

For biocompatibility, the upconversion nanoparticles were functionalized with TPGS ligands. The procedure was as follows: 100 mg of TPGS was dispersed in 10 mL of cyclohexane and activated at room temperature for 1 h. $NaYF_4$:Yb^{3+}/Er^{3+}@silica nanoparticles (200 mg) were dispersed in 15 mL of ethanol and then added dropwise into the activated TPGS solution and stirred for 60 min by a magnetic stirrer (solution 2). Then, 20 mL of deionized water was added to solution 2, and it was stirred continuously at 70 °C for 60 min to evaporate the cyclohexane. $NaYF_4$:Yb^{3+}/Er^{3+}@silica-TPGS bio-nano complexes could be obtained by centrifugation.

MCF-7 Breast Cancer Cell and HEK-293A Cell Culture and Fluorescence Imaging of Cells. In this study, the experiments were implemented on MCF-7 breast cancer cells and HEK-293A healthy cells, which were maintained in Eagle's Minimum Essential Medium (EMEM) with fetal bovine serum (10%) (Sigma) and gentamicin (50 μg/mL) at 37 °C and 5% CO_2 in a humidified atmosphere. The cells were seeded at a density of 5.10^4 cells/mL.[29] To study the uptake capacity of functionalized $NaYF_4$:Yb^{3+}/Er^{3+}@silica-TPGS, the MCF-7 breast cancer cells and HEK-293A cells (10^6 cells/mL) at log phase were seeded in 24-well plates and then incubated for 24 h. Poly(ethylene glycol) 1500 (Sigma) and $NaYF_4$:Yb^{3+}/Er^{3+}@silica/$NaYF_4$:Yb^{3+}/Er^{3+}@silica-TPGS nanoparticles (with a concentration of 20 μg/mL) were then added to the cell-seeded wells for 3 h. After the assigned time, the culture medium was discarded, and cells were harvested into 15 mL falcon tubes. The cell tubes were centrifuged at 1000 rpm for 5 min to thoroughly remove the culture medium. The cells were then washed with phosphate-buffered saline three times. At the end of the process, phosphate-buffered saline was added to the wells before and after MCF-7 breast cancer cells and HEK-293A cells were incubated with a $NaYF_4$:Yb^{3+}/Er^{3+}@silica or $NaYF_4$:Yb^{3+}/Er^{3+}@silica-TPGS bio-nano complex. The cell images were obtained using a fluorescence inverted microscope (ZEISS AXIOSCOPE A1) with 200× magnification.

Characterization. In this work, characterization of the sample structure was performed by an X-ray diffractometer using a Siemens D5000 with λ = 1.5406 Å. The morphology and the energy-dispersive X-ray spectra were observed and measured by a field emission scanning electron microscope (S-4800, Hitachi) and a high-resolution transmission electron microscope (JEM 2100, JEOL). The infrared absorption spectra were obtained employing a Fourier transform infrared spectrometer (L1600400 Spectrum Two FT-IR DTGS). The upconversion photoluminescence properties were studied using an iHR550 photoluminescence measurement system (Horiba) at an excitation of 980 nm.

RESULTS AND DISCUSSION

Structural and Morphological Characterization. Figure 1 shows the X-ray diffraction (XRD) pattern of the as-synthesized $NaYF_4$:Yb^{3+}/Er^{3+}, $NaYF_4$:Yb^{3+}/Er^{3+}@silica, and $NaYF_4$:Yb^{3+}/Er^{3+}@silica-TPGS. It can be observed that the diffraction peaks of the samples coincide well with the standard data of the hexagonal-phase $NaYF_4$ structure (JCPDS No. 28-1192). No impurity peaks are seen, indicating that the dopants Yb^{3+} and Er^{3+} are well dispersed in the host lattice. Furthermore, the hexagonal crystalline structure (β-$NaYF_4$) has a large gap between the two Er^{3+} ions, leading to reduced fluorescence quenching.[30,31] This is very beneficial for obtaining strong luminescence and its applications.

https://doi.org/10.1021/acs.jpcb.1c05472
J. Phys. Chem. B 2021, 125, 9768−9775

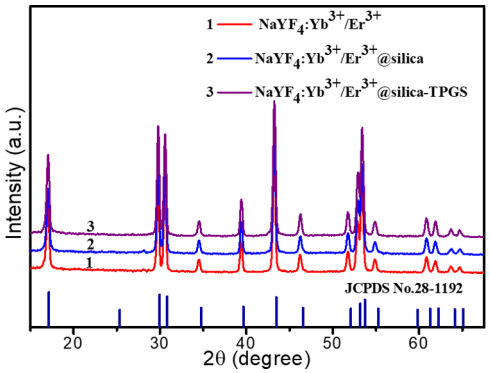

Figure 1. X-ray diffraction pattern of the nanoparticles $NaYF_4$:Yb^{3+}/Er^{3+}, $NaYF_4$:Yb^{3+}/Er^{3+}@silica, and $NaYF_4$:Yb^{3+}/Er^{3+}@silica-TPGS and the standard data of hexagonal-phase $NaYF_4$ (JCPDS No. 28-1192) as a reference.

Figure 2a–c shows the scanning electron microscopy (SEM) images of the nanoparticles $NaYF_4$:Yb^{3+}/Er^{3+}, $NaYF_4$:Yb^{3+}/Er^{3+}@silica, and $NaYF_4$:Yb^{3+}/Er^{3+}@silica-TPGS, respectively. It can be observed that $NaYF_4$:Yb^{3+}/Er^{3+} cores have a nearly spherical shape with a diameter of about 120–150 nm in Figure 2a. After the nanoparticles were covered with silica and functionalized with TPGS, their diameter is increased to 150–180 nm (Figure 2c). The diameter of particles is hundreds of nanometers as the basis for making extracellular probes and containing anticancer drugs (T-drug).[32,33] In addition, a high-resolution transmission electron microscopy (HRTEM) image of the nanoparticle $NaYF_4$:Yb^{3+}/Er^{3+}@silica-TPGS is shown in Figure 2d. It indicates that the $NaYF_4$:Yb^{3+}/Er^{3+} (~135 nm) core is coated with a silica–TPGS shell. The porous cavities on the surface can prevent quenching passivation of optically active ions in the core due to enhanced upconversion emission intensity.

Energy-Dispersive X-ray Analysis and Fourier Transform Infrared Spectra. The representative energy-dispersive X-ray (EDX) spectrum of the $NaYF_4$:Yb^{3+}/Er^{3+}@silica-TPGS nanoparticles is shown in Figure 3a. It shows the strong peaks of the main Na, Y, and F elements; two weaker Yb and Er peaks; and Si, O, and C peaks from the coating layer of silica and TPGS. This confirms that the silica shell and TPGS were successfully coated on the surface of the $NaYF_4$:Yb^{3+}/Er^{3+} core. It should be noted that the height of the Si, O, and C peaks may be attributed to a small number of impurities, probably dust.

Fourier transform infrared (FTIR) spectra of $NaYF_4$:Yb^{3+}/Er^{3+}, $NaYF_4$:Yb^{3+}/Er^{3+}@silica, and $NaYF_4$:Yb^{3+}/Er^{3+}@silica-TPGS were obtained as shown in Figure 3b, further confirming the particle surface modification. In the case of $NaYF_4$:Yb^{3+}/Er^{3+}@silica-TPGS nanoparticles, an absorption band at 1738 cm^{-1} is observed, which can be assigned to the carbonyl group (−C═O) of TPGS.[23,34] Overlapping of the −CH stretching band of TPGS is observed at 2925 cm^{-1}.[23,34] The prominent band at 1090 cm^{-1} corresponds to the Si−O asymmetric stretch. All of the spectra exhibit a broad band at about 3433 cm^{-1} due to the O−H stretching vibration.[35,36] The results indicate the formation of TPGS onto $NaYF_4$:Yb^{3+}/Er^{3+}@silica nanoparticles. The crucial condition for TPGS-coated nanoparticles is to close the cell inside the physiological environment both *in vitro* and *in vivo*.

Upconversion Photoluminescence Properties. Figure 4a shows the upconversion photoluminescence spectra of the $NaYF_4$:Yb^{3+}/Er^{3+} nanoparticles under a 980 nm continuous-wave (CW) laser with different excitation powers at room temperature. The spectra exhibit three broad emission bands from green to red centered at 520, 541, and 654 nm, which are

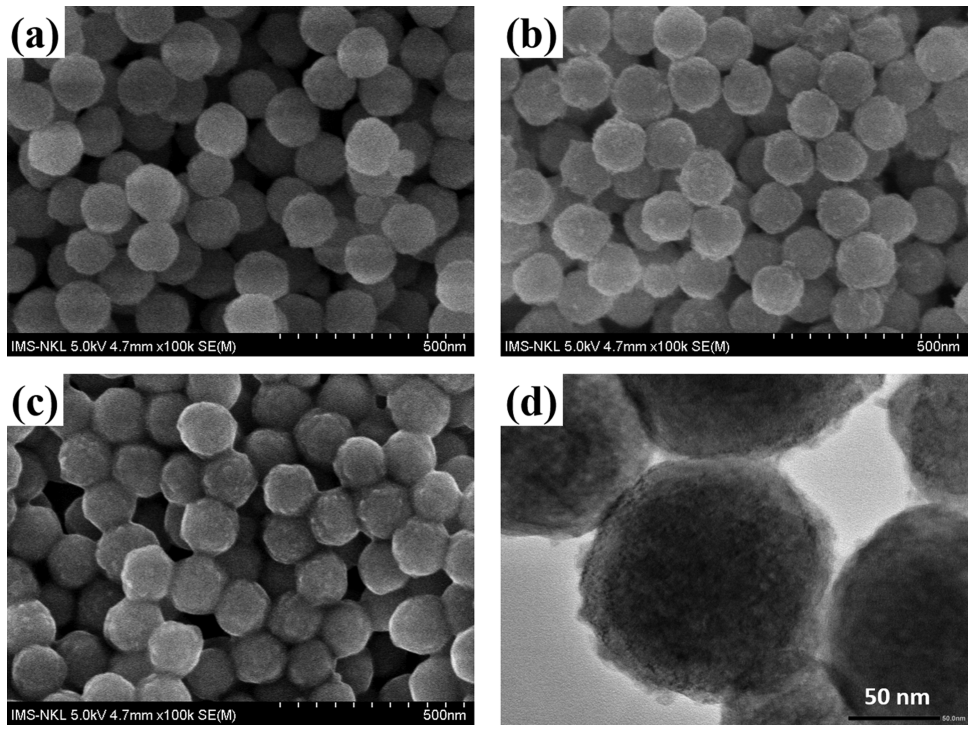

Figure 2. Morphological characterizations: (a–c) SEM images of the nanoparticles $NaYF_4$:Yb^{3+}/Er^{3+}, $NaYF_4$:Yb^{3+}/Er^{3+}@silica, and $NaYF_4$:Yb^{3+}/Er^{3+}@silica-TPGS, respectively. (d) HRTEM image of the nanoparticle $NaYF_4$:Yb^{3+}/Er^{3+}@silica-TPGS.

https://doi.org/10.1021/acs.jpcb.1c05472
J. Phys. Chem. B 2021, 125, 9768–9775

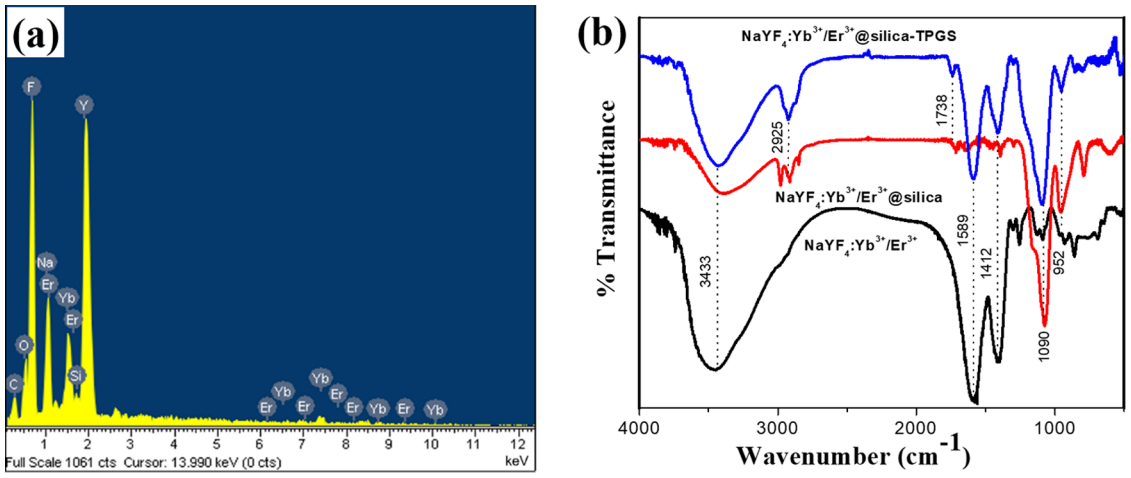

Figure 3. (a) EDX spectrum of the nanoparticle $NaYF_4$:Yb^{3+}/Er^{3+}@silica-TPGS. (b) FTIR spectra of the nanoparticles $NaYF_4$:Yb^{3+}/Er^{3+}, $NaYF_4$:Yb^{3+}/Er^{3+}@silica, and $NaYF_4$:Yb^{3+}/Er^{3+}@silica-TPGS.

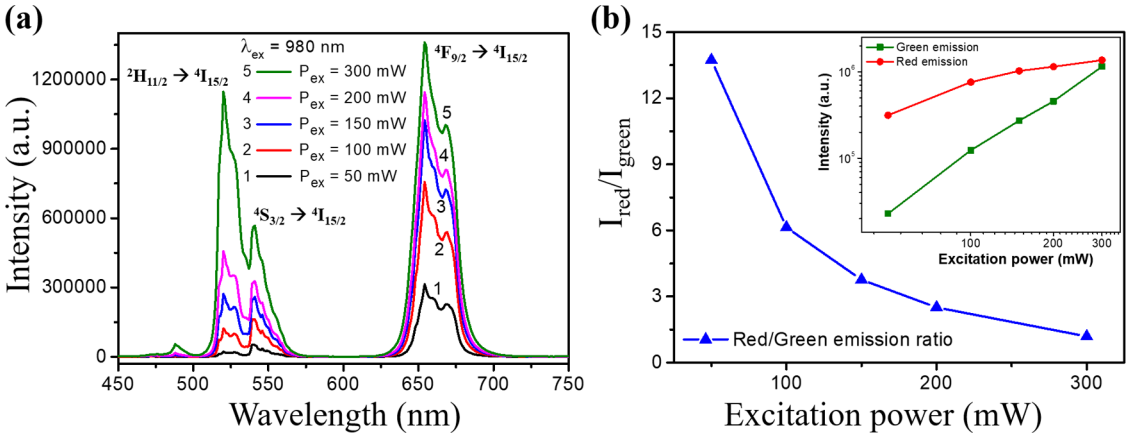

Figure 4. (a) Upconversion photoluminescence spectra of $NaYF_4$:Yb^{3+}/Er^{3+} nanoparticles at 980 nm with different excitation powers (50, 100, 150, 200, and 300 mW). (b) Dependence of the red-to-green emission intensity ratio on the excitation power of the sample; the inset presents the emission intensity of green (520 nm) and red (654 nm).

ascribed to the $^2H_{11/2} \rightarrow {}^4I_{15/2}$, $^4S_{3/2} \rightarrow {}^4I_{15/2}$, and $^4F_{9/2} \rightarrow {}^4I_{15/2}$ energy transitions in Er^{3+}, respectively.[37−39] When the excitation power is increased from 50 to 300 mW, the intensity of both red and green emissions is enhanced. However, the intensities are not proportional to excitation power, but the intensity of the green emission grows much faster than that of the red emission. Figure 4b shows the dependence of the red-to-green emission intensity ratio on excitation power, and the inset exhibits the emission intensity of green (520 nm) and red (654 nm). The emission ratio was calculated by dividing the emission intensity from the 654 nm peak by the emission intensity from the 520 nm peak, which decreases from 13.7 to 1.2 when the excitation power is increased from 50 to 300 mW. It is well known that upconversion is a nonlinear optical phenomenon in which the successive absorption of multi-photon leads to the emission luminescence at a shorter wavelength than the excitation wavelength. It is a distinct anti-Stokes process and can be achieved by incoherent excitation sources. Ground-state absorption (GSA), excited-state absorption (ESA), and energy transfer (ET) are three main mechanisms for upconversion.[37−39]

Figure 5 presents the energy-level diagram of Yb^{3+} and Er^{3+} ions and the corresponding upconversion mechanism of $NaYF_4$:Yb^{3+}/Er^{3+} nanoparticles. Because the Yb^{3+} ion has a

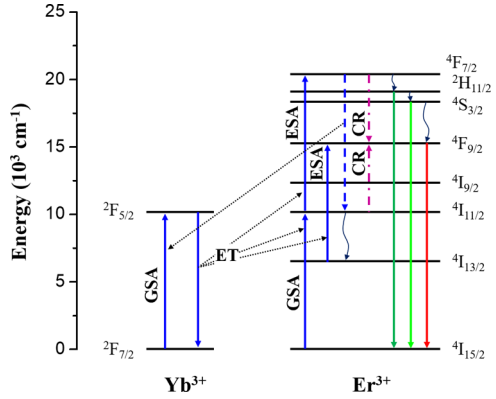

Figure 5. Energy-level diagram of Yb^{3+} and Er^{3+} ions and the proposed upconversion luminescence mechanism of the $NaYF_4$:Yb^{3+}/Er^{3+} nanoparticles.

larger absorption cross section at 980 nm, the ET process from Yb^{3+} to Er^{3+} is the main contribution to the upconversion luminescence. The Er^{3+} ions are first excited from the ground state $^4I_{15/2}$ to the $^4I_{11/2}$ level by the GSA (pumping photon) or ET ($^4I_{15/2}$(Er) + $^2F_{5/2}$ (Yb) → $^4I_{11/2}$(Er) + $^2F_{7/2}$ (Yb)) process and then to the $^4F_{7/2}$ level *via* the ESA or ET ($^4I_{11/2}$(Er) +

https://doi.org/10.1021/acs.jpcb.1c05472
J. Phys. Chem. B 2021, 125, 9768−9775

$^2F_{5/2}$ (Yb) → $^4I_{7/2}$(Er) + $^2F_{7/2}$ (Yb)) process. The Er^{3+} ions at the $^4F_{7/2}$ state could decay nonradiatively to the emitting $^2H_{11/2}$, $^4S_{3/2}$, and $^4F_{9/2}$ levels. The Er^{3+} ions at the $^4I_{11/2}$ level relax to the $^4I_{13/2}$ level and subsequently are excited to the $^4F_{9/2}$ state by the ESA or ET ($^4I_{13/2}$(Er) + $^2F_{5/2}$ (Yb) → $^4F_{9/2}$(Er) + $^2F_{7/2}$ (Yb)) process. Moreover, the cross-relaxation (CR) process between Er^{3+} ions could contribute to enhancing population density at the $^4F_{9/2}$ level. As shown in Figure 4, the energy gap between $^4F_{7/2}$ and $^4F_{9/2}$ (approximately 5150 cm^{-1}) matches well with the energy gap between $^4F_{9/2}$ and $^4I_{11/2}$.[40,41] Thus, the intensity of the red emission is stronger than that of the green emission owing to low excitation powers. However, when the pumping photon concentration increases to higher values, the leading two-photon absorptions are responsible and the ET process becomes more active to populate the excited levels. It can be deduced that the green emission intensity rises faster than the red emission intensity with increasing excitation powers. In fact, the strong red emission with low excitation powers is expected to be better than the green emission due to easier observation for *in vitro* experiments.

Figure 6 shows the photoluminescence spectra of the $NaYF_4$:Yb^{3+}/Er^{3+}, $NaYF_4$:Yb^{3+}/Er^{3+}@silica, and $NaYF_4$:Yb^{3+}/Er^{3+}@silica-TPGS nanoparticles in water suspension under 980 nm excitation.

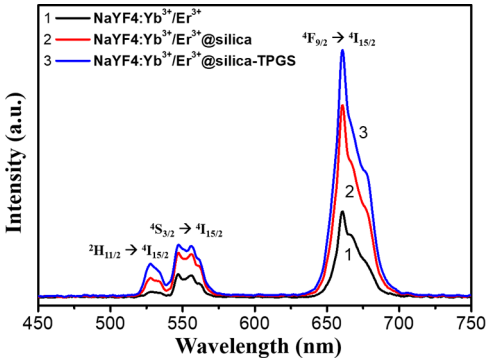

Figure 6. Upconversion photoluminescence spectra of the $NaYF_4$:Yb^{3+}/Er^{3+}, $NaYF_4$:Yb^{3+}/Er^{3+}@silica, and $NaYF_4$:Yb^{3+}/Er^{3+}@silica-TPGS nanoparticles in water suspension under 980 nm excitation.

Er^{3+}@silica-TPGS nanoparticles in water suspension at 980 nm excitation. The upconversion emission of $NaYF_4$:Yb^{3+}/Er^{3+} nanoparticles with typical energy transitions can be observed. However, a significant enhancement of the luminescence intensity was observed in $NaYF_4$:Yb^{3+}/Er^{3+}@silica-TPGS compared to that in $NaYF_4$:Yb^{3+}/Er^{3+} water emulsion. The red emission intensity of $NaYF_4$:Yb^{3+}/Er^{3+}@silica-TPGS is 2.9-fold higher than that of $NaYF_4$:Yb^{3+}/Er^{3+}. This enhancement can be explained by substitution of the O−H luminescence quenching with O═C and C−H.[42,43] The energy of the O═C and C−H stretching vibrations (1738, 2945 cm^{-1}) is lower than that of O−H (3400 cm^{-1}), which leads to a decrease in the multiphoton relaxation rate in the case of surface modification and enhancement of luminescence. Surface modification of the $NaYF_4$:Yb^{3+}/Er^{3+} nanoparticles with silica and TPGS not only improves their dispersibility in physiological media but also increases their upconversion photoluminescence intensity because coating layers can enhance the chemical stability and prevent RE ion leakage. This indicates that the $NaYF_4$:Yb^{3+}/Er^{3+}@silica-TPGS bio-nano complex can be used as a luminescent labeling material.

***In Vitro* Labeling of Cells.** In this set of experiments, MCF-7 breast cancer cells were incubated with $NaYF_4$:Yb^{3+}/Er^{3+}@silica-TPGS bio-nano complexes. It is well known that the cell membrane is always negatively charged.[44,45] So, the $NaYF_4$:Yb^{3+}/Er^{3+}@silica-TPGS bio-nano complexes are active particles with positive charges owing to the dangling bond of Yb^{3+}/Er^{3+} on the surface of particles, which should be able to bind with the membrane of MCF-7 breast cancer cells. Localization of the particles on the cell's surface was demonstrated by a fluorescence microscope under 980 nm excitation. Three fluorescence images of the MCF-7 breast cancer cells were obtained without/with $NaYF_4$:Yb^{3+}/Er^{3+}@silica and $NaYF_4$:Yb^{3+}/Er^{3+}@silica-TPGS in the cases of bright field, dark field, and merged modes as shown in Figure 7a−c,

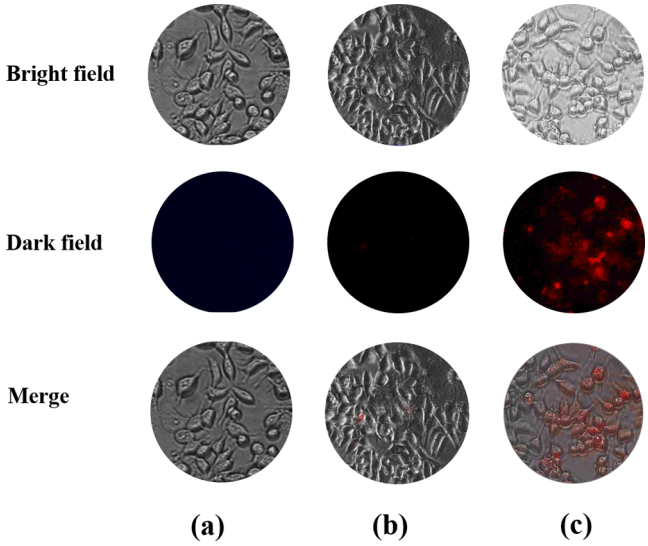

Figure 7. Fluorescence images of (a) MCF-7 breast cancer cells, (b) MCF-7 breast cancer cells after incubation with $NaYF_4$:Yb^{3+}/Er^{3+}@silica, and (c) MCF-7 breast cancer cells after incubation with $NaYF_4$:Yb^{3+}/Er^{3+}@silica-TPGS bio-nano complexes with different modes.

respectively. This indicates that we can only observe a typical MCF-7 breast cancer cell with/without $NaYF_4$:Yb^{3+}/Er^{3+}@silica and $NaYF_4$:Yb^{3+}/Er^{3+}@silica-TPGS in the bright field mode, whereas in the dark field mode, the $NaYF_4$:Yb^{3+}/Er^{3+}@silica-TPGS nanoparticles are significantly enhanced as shown by the localization image in the cells due to upconversion emission. The merged images show clearly that the $NaYF_4$:Yb^{3+}/Er^{3+}@silica-TPGS bio-nano complexes have adhered around the MCF-7 breast cancer cells. The presence of the $NaYF_4$:Yb^{3+}/Er^{3+}@silica-TPGS bio-nano complexes in the MCF-7 breast cancer cells is proven.

Surprisingly, the nanocomplex exhibited much fewer probing activities on HEK-293A human embryonic kidney cells, which were noncancerous cell lines. Figure 8a−c shows the fluorescence images of the HEK-293A cells without/with $NaYF_4$:Yb^{3+}/Er^{3+}@silica and $NaYF_4$:Yb^{3+}/Er^{3+}@silica-TPGS. The experimental conditions were the same as those for the MCF-7 breast cancer cells, and the images were taken in the cases of bright field, dark field, and merged modes. $NaYF_4$:Yb^{3+}/Er^{3+}@silica and $NaYF_4$:Yb^{3+}/Er^{3+}@silica-TPGS could not probe healthy cells of HEK-293A.

The cancerous typical labeling of $NaYF_4$:Yb^{3+}/Er^{3+}@silica-TPGS bio-nano complexes could come from the TPGS component. As reported elsewhere, TPGS in combination with other drugs leads to robust effects due to its capacity to

https://doi.org/10.1021/acs.jpcb.1c05472
J. Phys. Chem. B 2021, 125, 9768−9775

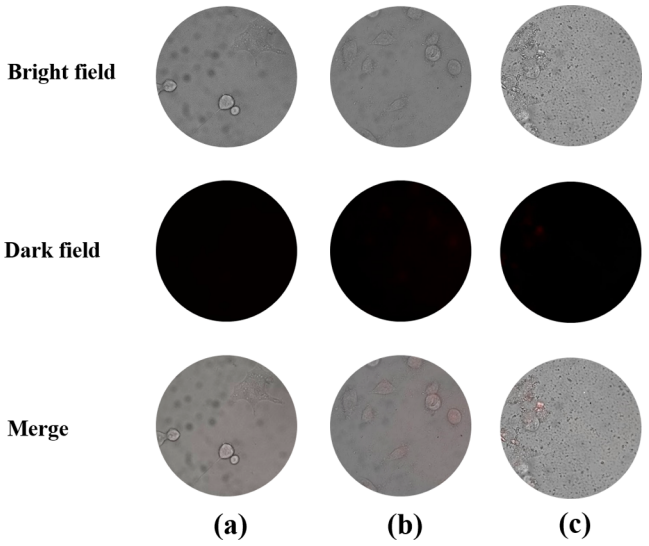

Figure 8. Fluorescence images of (a) HEK-293A embryonic kidney cells, (b) HEK-293A embryonic kidney cells after incubation with $NaYF_4$:Yb^{3+}/Er^{3+}@silica, and (c) HEK-293A embryonic kidney cells after incubation with $NaYF_4$:Yb^{3+}/Er^{3+}@silica-TPGS bio-nano complexes with different modes.

inhibit P-glycoprotein, an ATP-dependent drug efflux pump, as well as multidrug resistance protein 1 (MDR1) or ATP-binding cassette subfamily B member 1 (ABCB1) of cancer cells.[46] Also, as a single agent, TPGS has been found to inhibit the growth of the human lung, prostate, and breast cancer cells by inducing apoptosis.[47] Thus, as a component of this nano-conjugation, TPGS seems to have some effects on cancer cell surface markers, leading to a more specific labeling capacity of the $NaYF_4$:Yb^{3+}/Er^{3+}@silica-TPGS bio-nano complexes rather than normal immortalized HEK-293A cells. As reported, TPGS can also induce the programmed cell death of T-cell acute lymphocytic leukemia Jurkat clone E6-1 cells but not human peripheral blood lymphocytes, coincidentally.[48] The selective apoptosis-induced mechanisms of cancer cells mediated by TPGS are complicated and can be listed as a reactive oxygen species (ROS) inducer, downregulation of antiapoptotic proteins, and/or DNA damage. As long as cancer cells were induced to apoptotic states, a major change of cell membranes and surface markers was recorded. This might explain the $NaYF_4$:Yb^{3+}/Er^{3+}@silica-TPGS's specific labeling capacity on MCF-7 cancer cells rather than nontumorigenic HEK-293A cells in this experiment. This approach allows us to determine the biodistribution of the nanoparticles and has great potential for labeling in biological applications.

CONCLUSIONS

Well-crystallized $NaYF_4$:Yb^{3+}/Er^{3+} nanoparticles were synthesized *via* a hydrothermal method, further protected with a silica shell by the modified Stöber method, and functionalized with TPGS. The $NaYF_4$:Yb^{3+}/Er^{3+} nanoparticles exhibit strong upconversion luminescence by a nonlinear optical process, including a green emission band at 520 nm and a predominant red emission band at 654 nm. The experimental result indicates that surface modification of $NaYF_4$:Yb^{3+}/Er^{3+} nanoparticles not only improves their dispersibility in physiological media but also increases their upconversion emission intensity. We demonstrated that $NaYF_4$:Yb^{3+}/Er^{3+}@silica-TPGS can typically probe MCF-7 breast cancer cells but could not detect HEK-293A healthy cells for *in vitro* experiments. This newly found result is supposed to be caused by the TPGS component. The $NaYF_4$:Yb^{3+}/Er^{3+}@silica-TPGS bio-nano complexes with significant biocompatibility provide a strong red upconversion emission upon very low excitation power, which has the potential to be an ideal nanoparticle for labeling and detecting in biomedical applications.

AUTHOR INFORMATION

Corresponding Author

Tran Thu Huong − *Institute of Materials Science, Vietnam Academy of Science and Technology, Hanoi 100000, Vietnam; Graduate University of Science and Technology, Vietnam Academy of Science and Technology, Hanoi 100000, Vietnam;* orcid.org/0000-0003-3556-6293; Email: huongtt.ims@gmail.com, huongtt@ims.vast.ac.vn

Authors

Ha Thi Phuong − *Hanoi Medical University, Hanoi 100000, Vietnam*

Le Thi Vinh − *Hanoi University of Mining and Geology, Hanoi 100000, Vietnam*

Hoang Thi Khuyen − *Institute of Materials Science, Vietnam Academy of Science and Technology, Hanoi 100000, Vietnam; Graduate University of Science and Technology, Vietnam Academy of Science and Technology, Hanoi 100000, Vietnam*

Do Thi Thao − *Institute of Biotechnology, Vietnam Academy of Science and Technology, Hanoi 100000, Vietnam*

Le Dac Tuyen − *Hanoi University of Mining and Geology, Hanoi 100000, Vietnam*

Tran Kim Anh − *Institute of Theoretical and Applied Research, Duy Tan University, Hanoi 100000, Vietnam*

Le Quoc Minh − *Institute of Theoretical and Applied Research, Duy Tan University, Hanoi 100000, Vietnam*

Complete contact information is available at: https://pubs.acs.org/10.1021/acs.jpcb.1c05472

Author Contributions

T.T.H., H.T.P., and L.T.V. conceived the idea and designed the experiments. T.T.H., H.T.P., L.T.V., H.T.K., T.K.A., and D.T.T. conducted most of the experiments. All authors contributed to data analysis and interpretation and discussed the results. T.T.H., D.T.T., L. D.T., and L.Q.M. contributed to writing the manuscript. The manuscript was written through contributions of all authors. All authors have given approval to the final version of the manuscript.

Notes

The authors declare no competing financial interest.

ACKNOWLEDGMENTS

This research was funded by the Vietnam National Foundation for Science and Technology Development (NAFOSTED) under Grant Number 103.03-2017.66.

ABBREVIATIONS

TPGS, D-α-tocopheryl polyethylene glycol 1000 succinate; MCF-7, breast cancer cells; HEK-293A, human embryonic kidney cells; RE, rare earth; XRD, X-ray diffraction; EDX, energy-dispersive X-ray; SEM, scanning electron microscopy; HRTEM, high-resolution transmission electron microscopy;

https://doi.org/10.1021/acs.jpcb.1c05472
J. Phys. Chem. B 2021, 125, 9768−9775

FTIR, Fourier transform infrared; GSA, ground-state absorption; ESA, excited-state absorption; ET, energy transfer

REFERENCES

(1) Hu, Z.; Fang, C.; Li, B.; Zhang, Z.; Cao, C.; Cai, M.; Su, S.; Sun, X.; Shi, X.; Li, C.; et al. First-in-human liver-tumour surgery guided by multispectral fluorescence imaging in the visible and near-infrared-I/II windows. *Nat. Biomed. Eng.* **2020**, *4*, 259−271.

(2) Niekamp, S.; Stuurman, N.; Vale, R. D. A 6-nm ultra-photostable DNA FluoroCube for fluorescence imaging. *Nat. Methods* **2020**, *17*, 437−441.

(3) Li, C.; Chen, G.; Zhang, Y.; Wu, F.; Wang, Q. Advanced Fluorescence Imaging Technology in the Near-Infrared-II Window for Biomedical Applications. *J. Am. Chem. Soc.* **2020**, *142*, 14789−14804.

(4) Zhou, Y.; Zhang, D.; He, G.; Liu, C.; Tu, Y.; Li, X.; Zhang, Q.; Wu, X.; Liu, R. A lysosomal targeted NIR photosensitizer for photodynamic therapy and two-photon fluorescence imaging. *J. Mater. Chem. B* **2021**, *9*, 1009−1017.

(5) Wei, Y.; Liu, Y.; He, Y.; Wang, Y. Mitochondria and lysosome-targetable fluorescent probes for hydrogen peroxide. *J. Mater. Chem. B* **2021**, *9*, 908−920.

(6) DaCosta, M. V.; Doughan, S.; Han, Y.; Krull, U. J. Lanthanide upconversion nanoparticles and applications in bioassays and bioimaging: A review. *Anal. Chim. Acta* **2014**, *832*, 1−33.

(7) Zhou, J.; Liu, Q.; Feng, W.; Sun, Y.; Li, F. Upconversion luminescent materials: Advances and applications. *Chem. Rev.* **2015**, *115*, 395−465.

(8) Zhou, M.; Ge, X.; Ke, D. M.; Tang, H.; Zhang, J. Z.; Calvaresi, M.; Gao, B.; Sun, L.; Su, Q.; Wang, H. The Bioavailability, Biodistribution, and Toxic Effects of Silica-Coated Upconversion Nanoparticles *in vivo*. *Front. Chem.* **2019**, *7*, No. 218.

(9) Jia, F.; Li, G.; Yang, B.; Yu, B.; Shen, Y.; Cong, H. Investigation of rare earth upconversion fluorescent nanoparticles in biomedical field. *Nanotechnol. Rev.* **2019**, *8*, 1−17.

(10) Wilhelm, S.; Kaiser, M.; Würth, C.; Heiland, J.; Carrillo-Carrion, C.; Muhr, V.; Wolfbeis, O. S.; Parak, W. J.; Resch-Genger, U.; Hirsch, T. Water dispersible upconverting nanoparticles: effects of surface modification on their luminescence and colloidal stability. *Nanoscale* **2015**, *7*, 1403−1410.

(11) Feng, W.; Zhu, X.; Li, F. Recent advances in the optimization and functionalization of upconversion nanomaterials for *in vivo* bioapplications. *NPG Asia Mater.* **2013**, *5*, No. e75.

(12) Chávez-García, D.; Moreno, K. J.; Campos, C. H.; Alderete, J.; Hirata, G. Upconversion rare earth nanoparticles functionalized with folic acid for bioimaging of MCF-7 breast cancer cells. *J. Mater. Res.* **2018**, *33*, 191−200.

(13) Zhou, B.; Shi, B.; Jin, D.; Liu, X. Controlling upconversion nanocrystals for emerging applications. *Nat. Nanotechnol.* **2015**, *10*, 924−936.

(14) Huang, M.; Wang, L.; Zhang, X.; Zhou, J.; Liu, L.; Pan, Y.; Yu, B.; Yu, Z. Synthesis and Characterization of Folic Acid Labeled Upconversion Fluorescent Nanoprobes for *in vitro* Cancer Cells Targeted Imaging. *Nano* **2017**, *12*, No. 1750057.

(15) Chen, G.; Ågren, H.; Ohulchanskyy, T. Y.; Prasad, P. N. Light upconverting core−shell nanostructures: nanophotonic control for emerging applications. *Chem. Soc. Rev.* **2015**, *44*, 1680−1713.

(16) Kaczmarek, A. M.; Kaczmarek, M. K.; Deun, R. V. Er^{3+}-to-Yb^{3+} and Pr^{3+}-to-Yb^{3+} energy transfer for highly efficient near-infrared cryogenic optical temperature sensing. *Nanoscale* **2019**, *11*, 833−837.

(17) Kamińska, I.; Wosztyl, A.; Kowalik, P.; Sikora, B.; Wojciechowski, T.; Sobczak, K.; Minikayev, R.; Zajdel, K.; Chojnacki, M.; Zaleszczyk, W.; et al. Synthesis and characterization of Gd_2O_3: Er^{3+}, Yb^{3+} doped with Mg^{2+}, Li^+ ions - effect on the photoluminescence and biological applications. *Nanotechnology* **2021**, *32*, No. 245705.

(18) Min, B. H.; Youl, K. J. Enhanced upconversion luminescence of $GdVO_4$:Er^{3+}/Yb^{3+} prepared by spray pyrolysis using organic additives. *RSC Adv.* **2019**, *9*, 20002−20008.

(19) Krut'ko, V. A.; Komova, M. G.; Pominova, D. V.; Nikiforova, G. E. Enhanced red up-conversion luminescence in $La_{4-x-y}Gd_{10}Ge_2B_6O_{34}$:$Yb_x$, Er_y synthesized by the liquid-phase homogenization with tartaric acid. *J. Sol-Gel Sci. Technol.* **2019**, *92*, 442−448.

(20) Van Phan, D.; Quang, V. X.; Tuyen, H. V.; Ngoc, T.; Tuyen, V. P.; Thanh, L. D.; Ca, N. X.; Hien, N. T. Structure, optical properties and energy transfer in potassium-alumino-borotellurite glasses doped with Eu^{3+} ions. *J. Lumin.* **2019**, *216*, No. 116748.

(21) Xie, J.; Hu, W.; Tian, D.; Wei, Y.; Zheng, G.; Huang, L.; Liang, E. Selective growth and upconversion photoluminescence of Y-based fluorides: from $NaYF_4$: Yb/Er to YF_3: Yb/Er crystals. *Nanotechnology* **2020**, *31*, No. 505605.

(22) Yang, C.; Wu, T.; Qi, Y.; Zhang, Z. Recent Advances in the Application of Vitamin E TPGS for Drug Delivery. *Theranostics* **2018**, *8*, 464−485.

(23) Khare, V.; Sakarchi, W. A.; Gupta, P. N.; Curtis, A. D. M.; Hoskins, C. Synthesis and characterization of TPGS−gemcitabine prodrug micelles for pancreatic cancer therapy. *RSC Adv.* **2016**, *6*, 60126−60137.

(24) Puig-Rigall, J.; Blanco-Prieto, M. J.; Radulescu, A.; Dreiss, C. A.; González-Gaitano, G. Morphology, gelation and cytotoxicity evaluation of D-α-Tocopheryl polyethylene glycol succinate (TPGS) - Tetronic mixed micelles. *J. Colloid Interface Sci.* **2021**, *582*, 353−363.

(25) Hu, H.; Xiong, L.; Zhou, J.; Li, F.; Cao, T.; Huang, C. Multimodal-Luminescence Core-Shell Nanocomposites for Targeted Imaging of Tumor Cells. *Chem. - Eur. J.* **2009**, *15*, 3577−3584.

(26) Huong, T. T.; Vinh, L. T.; Anh, T. K.; Khuyen, H. T.; Phuong, H. T.; Minh, L. Q. Fabrication and Optical characterization of multimorphological nanostructured materials containing Eu(III) in phosphate matrices for biomedical application. *New J. Chem.* **2014**, *38*, 2114−2119.

(27) Wang, X.; Xu, T.; Bu, Y.; Yan, X. Giant enhancement of upconversion emission in $NaYF_4$: Er^{3+}@$NaYF_4$:Yb^{3+} active-core/active-shell nanoparticles. *RSC Adv.* **2016**, *6*, 22845−22851.

(28) Rinkel, T.; Raj, A. N.; Dühnen, S.; Haase, M. Synthesis of 10 nm β-$NaYF_4$:Yb,Er/$NaYF_4$ Core/Shell Upconversion Nanocrystals with 5 nm Particle Cores. *Angew. Chem., Int. Ed.* **2016**, *55*, 1164−1167.

(29) Phuong, H. T.; Huong, T. T.; Khuyen, H. T.; Vinh, L. T.; Thao, D. T.; Huong, N. T.; Lien, P. T.; Minh, L. Q. Synthesis and structural characterization of $NaYF_4$:Yb^{3+}, Er^{3+}@silica-N=Folic acide nanophosphors for bioimaging. *J. Rare Earths* **2019**, *37*, 1183−1187.

(30) Wang, J.; Song, H.; Xu, W.; Dong, B.; Xu, S.; Chen, B.; Yu, W.; Zhang, S. Phase transition, size control and color tuning of $NaREF_4$:Yb^{3+}, Er^{3+} (RE = Y, Lu) nanocrystals. *Nanoscale* **2013**, *5*, 3412−3420.

(31) Ding, M.; Yin, S.; Ni, Y.; Lu, C.; Chen, D.; Zhong, J.; Ji, Z.; Xu, Z. Controlled synthesis of β-$NaYF_4$:Yb^{3+}/Er^{3+} microstructures with morphology-and size dependent up conversion luminescence. *Ceram. Int.* **2015**, *41*, 7411−7420.

(32) He, L.; Xu, J.; Cheng, X.; Sun, M.; Wei, B.; Xiong, N.; Song, J.; Wang, X.; Tang, R. Hybrid micelles based on Pt (IV) polymeric prodrug and TPGS for the enhanced cytotoxicity in drug-resistant lung cancer cells. *Colloids Surf., B* **2020**, *195*, No. 111256.

(33) Ungun, B.; Prud'homme, R. K.; Budijono, S. J.; Shan, J.; Lim, S. F.; Ju, Y.; Austin, R. Nanofabricated upconversion nanoparticles for photodynamic therapy. *Opt. Express* **2009**, *17*, 80−86.

(34) Sonali; Agrawal, P.; Singh, R. P.; Rajesh, C. V.; Singh, S.; Vijayakumar, M. R.; Pandey, B. L.; Muthu, M. S. Transferrin receptor-targeted vitamin E TPGS micelles for brain cancer therapy: preparation, characterization and brain distribution in rats. *Drug Delivery* **2016**, *23*, 1788−1798.

(35) Tian, G.; Zheng, X.; Zhang, X.; Yin, W.; Yu, J.; Wang, D.; Zhang, Z.; Yang, X.; Gu, Z.; Zhao, Y. TPGS-stabilized $NaYbF_4$:Er upconversion nanoparticles for dual-modal fluorescent/CT imaging and anticancer drug delivery to overcome multi-drug resistance. *Biomaterials* **2015**, *40*, 107−116.

https://doi.org/10.1021/acs.jpcb.1c05472
J. Phys. Chem. B 2021, 125, 9768−9775

(36) Geitenbeek, R. G.; Prins, P. T.; Albrecht, W.; Blaaderen, A. V.; Weckhuysen, B. M.; Meijerink, A. $NaYF_4:Er^{3+},Yb^{3+}/SiO_2$ Core/Shell Upconverting Nanocrystals for Luminescence Thermometry up to 900 K. *J. Phys. Chem. C* **2017**, *121*, 3503−3510.
(37) Ding, Y.; Yang, T.; Yin, N.; Shu, F.; Zhao, Y.; Zhang, X. Synthesis of novel branched β-$NaLuF_4$: Yb/Er upconversion luminescence material and investigation of its optical properties. *Opt. Mater.* **2018**, *79*, 408−412.
(38) Gunaseelan, M.; Yamini, S.; Kumar, G. A.; Senthilselvan, J. Highly efficient upconversion luminescence in hexagonal $NaYF_4:Yb^{3+}$, Er^{3+} nanocrystals synthesized by a novel reverse microemulsion method. *Opt. Mater.* **2018**, *75*, 174−186.
(39) Giang, L. T. K.; Marciniak, L.; Hreniak, D.; Anh, T. K.; Minh, L. Q. Synthesis, Structural Characterization, and Emission Properties of $NaYF_4:Er^{3+}/Yb^{3+}$ Upconversion Nanoluminophores. *J. Electron Mater.* **2016**, *45*, 4790−4795.
(40) Cockroft, N. J.; Jones, G. D.; Nguyen, D. C. Dynamics and spectroscopy of infrared-to-visible upconversion in erbium-doped cesium cadmium bromide ($CsCdBr^3:Er^{3+}$). *Phys. Rev. B* **1992**, *45*, 5187−5198.
(41) Tang, J.; Sun, M.; Huang, Y.; Gou, J.; Zhang, Y.; Li, G.; Li, Y.; Man, Y.; Yang, J. Study on optical properties and upconversion luminescence of Er^{3+}/Yb^{3+} co-doped tellurite glass for highly sensitive temperature measuring. *Opt. Mater. Express* **2017**, *7*, 3238−3250.
(42) Feng, Y.; Li, Z.; Li, Q.; Yuan, J.; Tu, L.; Ning, L.; Zhang, H. Internal OH^- induced cascade quenching of upconversion luminescence in $NaYF_4$:Yb/Er nanocrystals. *Light: Sci. Appl.* **2021**, *10*, No. 105.
(43) Liu, Y.; Tu, D.; Zhu, H.; Chen, X. Lanthanide-doped luminescent nanoprobes: controlled synthesis, optical spectroscopy, and bioapplications. *Chem. Soc. Rev.* **2013**, *42*, 6924−6958.
(44) Li, Z.; Miao, H.; Fu, Y.; Liu, Y.; Zhang, R.; Tang, B. Fabrication of $NaYF_4$:Yb,Er Nanoprobes for Cell Imaging Directly by Using the Method of Hydrion Rivalry Aided by Ultrasonic. *Nanoscale Res. Lett.* **2016**, *11*, No. 441.
(45) Rascol, E.; Devoisselle, J. M.; Chopineau, J. The relevance of membrane models to understand nanoparticles−cell membrane interactions. *Nanoscale* **2016**, *8*, 4780−4798.
(46) Neophytou, C. M.; Mesaritis, A.; Gregoriou, G.; Constantinou, A. I. D-a-Tocopheryl Polyethylene Glycol 1000 Succinate and a small-molecule Survivin suppressant synergistically induce apoptosis in SKBR3 breast cancer cells. *Sci. Rep.* **2019**, *9*, No. 14375.
(47) Youk, H. J.; Lee, E.; Choi, M. K.; Lee, Y. J.; Chung, J. H.; Kim, S. H.; Lee, C. H.; Lim, S. J. Enhanced anticancer efficacy of alpha-tocopheryl succinate by conjugation with polyethylene glycol. *J. Controlled Release* **2005**, *107*, 43−52.
(48) Yang, C.; Wu, T.; Qi, Y.; Zhang, Z. Recent Advances in the Application of Vitamin E TPGS for Drug Delivery. *Theranostics* **2018**, *8*, 464−485.

https://doi.org/10.1021/acs.jpcb.1c05472
J. Phys. Chem. B 2021, 125, 9768−9775